Journal of Non-Newtonian Fluid Mechanics, 44 (1992) 127–148
Elsevier Science Publishers B.V., Amsterdam

Understanding cusped interfaces

Daniel D. Joseph

University of Minnesota, Department of Aerospace Engineering & Mechanics, Institute of Technology, 107 Akerman Hall, 110 Union Street S.E. Minneapolis, MN 55455 (USA)

(Received October 7, 1991)

Abstract

The good progress made on the recently opened problem of two-dimensional cusped interfaces in Newtonian and non-Newtonian fluids is reviewed. Some new results are presented and open problems are discussed.

Keywords: analytic cusp; disjoining pressure; Stokes flow singularity; surface tension

1. Experiments of Joseph, Nelson, Renardy and Renardy (JNRR) [1]

Two-dimensional cusped interfaces are line singularities of curvature. JNRR created such cusps in an experiment [1] by rotating a cylinder half immersed in liquid. A liquid film is dragged out of the reservoir on one side and is plunged in the other, where it forms a cusp at finite speeds, if the conditions are right. Both Newtonian and non-Newtonian fluids form cusps, but the transition from a rounded interface to a cusp is gradual in Newtonian liquids and sudden in non-Newtonian liquids. They presented striking photographs of the two-dimensional cusps on the free surface in regions of convergence of the flow to what would otherwise be a stagnation line. Jeong and Moffatt (hereafter JM) [2] repeated these experiments for one Newtonian fluid and also found critical conditions in which simple visual observation indicates the presence of a very sharp cusp. They noted that "... if powder is sprinkled on the free surface, this powder is immediately swept through the cusp into the interior of the fluid. Thus, observa-

Correspondence to: Dept. of Aerospace Engineering and Mechanics, Institute of Technology, 107 Akerman Hall, 110 Union Street S.E. Minneapolis, MN 55455 (USA).

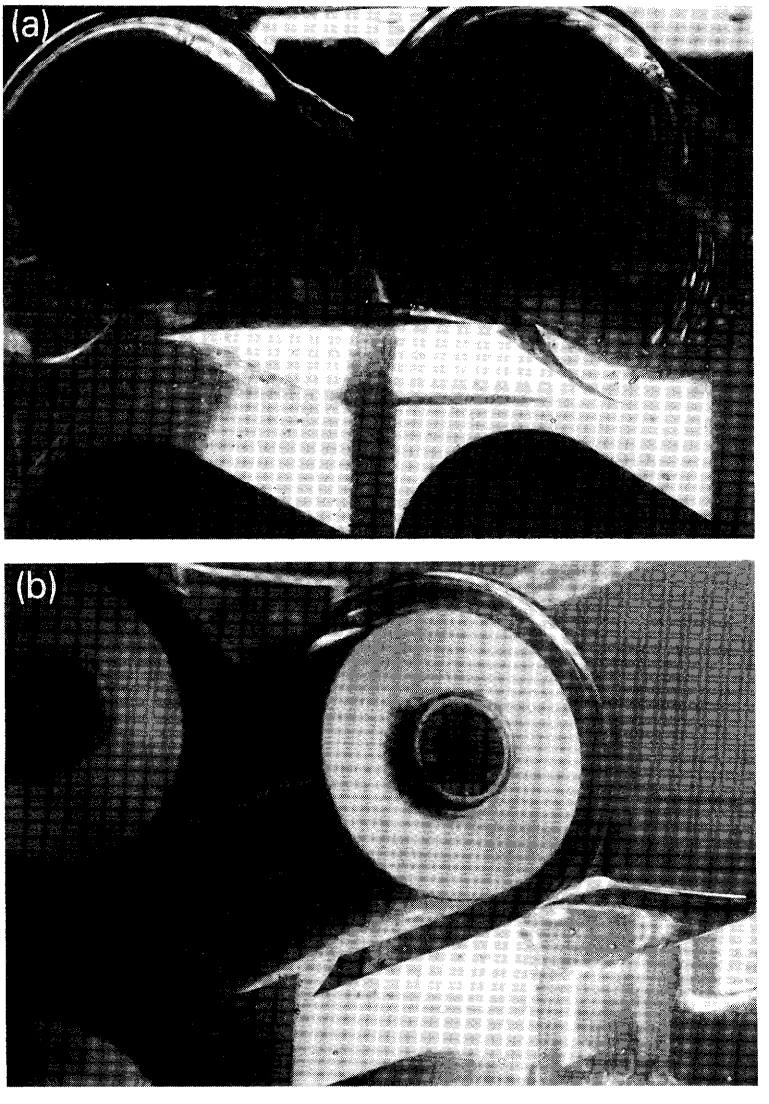

Fig. 1. Cylinder coated with TLA 510 cusps in air. (a) Liquid is dragged down between the cylinders, (b) liquid is dragged up between the cylinders.

tion suggests that fluid particles on the free surface are similarly advected through the cusp into the interior."

In Fig. 1 we have displayed photographs of two-dimensional cusped interfaces of TLA 510 (polyisobutylene in petroleum oil) in air. The speed at which the fluid passes the stationary cusp is called U and $U \approx \Omega a$ where Ω is the steady speed of rotation of the cylinder of radius $R < a$, a is the

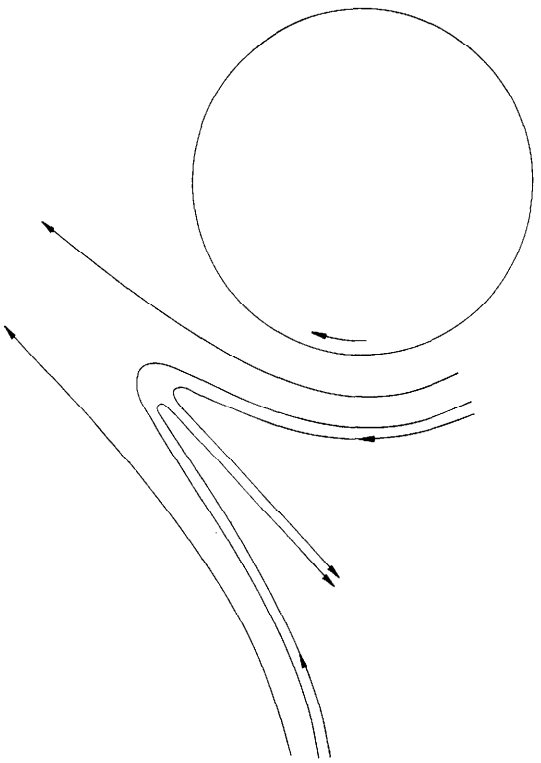

Fig. 2. Distorted interface in a two-liquid system. The point A is a stagnation point or a cusp. Where $\Omega = 0$, each fluid covers one-half of the cylinder.

distance from the cusp point to the cylinder center. When Ω is small there is no cusp, the free surface is rounded and the point of incipient cusping is actually a stagnation point with $U = 0$, as shown in Fig. 2.

2. Critical capillary numbers

There is a critical condition for cusping which appears to correlate with a capillary number

$$Ca = \mu U/\sigma,$$

where μ is the viscosity and σ is the surface tension.

Table 1 gives capillary numbers for some Newtonian and non-Newtonian fluids. For non-Newtonian fluids, the critical value of the rotation speed is very distinct. Below this value the interface is round. At the critical speed the interface suddenly transforms to a cusp. The critical speed is not distinct for those Newtonian fluids for which a cusp was observed. At slow

TABLE 1

Critical annular velocity and Ca_c values for the formation of a cusp

System	Critical angular velocity (rev min^{-1})	Critical radius (cm)	Ca_c
Newtonian fluids			
Castor oil	113	1.78	4.89
Glycerin	128	1.49	2.62
Silicone oil-500cs	75	1.64	2.96
Silicone oil-1000cs	41	1.40	2.75
Silicone oil-5000cs	26	1.57	8.21
SAE30 motor oil–Water	51	1.61	2.57
Non-Newtonian Fluids			
Honey	5.58	1.92	1.78
Polyox (1%)	52	1.35	9.24
Polyox (2%)	0.8	1.97	2.10
Silicone oil-12500cs	3.0	1.50	2.64
M1	2.4	1.90	0.48
STP	2.9	1.80	2.24

speeds the interface is round. As the rotation speed increases, the shape of the interface changes from rounded to pointed in a continuous manner, until at what we define as the critical speed the interface appears to be a cusp. The critical values for Newtonian liquids are a little ambiguous, but did not vary by more than 5% in different determinations. Once a cusp is formed, further increases in the angular velocity will only lengthen the cusp or end in an instability characterized by fingering.

JNRR also presented a list of Newtonian liquids which did not cusp. The capillary numbers for these fluids at the highest angular velocity, 128 rev min^{-1}, in Table 1 are listed in Table 2.

The results shown in Table 2 are consistent with the idea that all Newtonian liquids will cusp at capillary numbers exceeding those in Table 2, say at $Ca \approx 2.5$, if turbulence be suppressed. In fact, I could not test this

TABLE 2

Capillary numbers at 128 rev min^{-1} of liquids which did not cusp

Fluid	Ca
SAE 30 motor oil	1.60
Safflower oil	0.41
Silicone oil-200cs	1.86
Soybean oil	0.38

idea because the apparatus used by JNRR would not rotate at angular velocities much in excess of 200 rev min^{-1}.

3. Questions posed by the experiments

- Is there a real cusp, or just an apparent cusp with a rounded end with rounding that is too small to see?
- Arcs of a cusp, or an apparent cusp come close together. Is it necessary to take into account short-range forces, like Van der Waals forces, to get a correct description of cusping near the apparent tip of the cusp?
- Can the appearance of a cusp, or an apparent cusp, in a Newtonian liquid be correlated with a capillary number alone? Why does the cusping appear to occur at different capillary numbers in the neighborhood of 2.5?
- It is a great surprise that a critical capillary number for cusping, a parameter which should be important for Newtonian liquids, is evidently also relevant for the critical cusping in non-Newtonian liquids where extensional effects should be important. Is the capillary number $U\mu/\sigma$ really an important parameter for cusping in non-Newtonian fluids and how does it enter into cusping dynamics?
- Is the observed difference between cusping in Newtonian and non-Newtonian liquids qualitative or only quantitative. Could the sudden transition to cusping in a non-Newtonian fluid be described as an instability of stagnation point flow at a free surface?

4. The generic analytic cusp

Local analysis of a cusp in a Newtonian liquid must be framed in terms of Stokes flow, because the infinite curvature implies singular stresses so that the higher derivatives in stress terms will overwhelm inertia. This was pointed out by Richardson [3]. When I first became aware that cusping is a threshold phenomenon, I reasoned that the cusp shape ought to arise from an analytic solution that certainly would be generated from a highly elliptic problem governed by the biharmonic equation. This kind of reasoning leads to the cusp shape $y = cx^{3/2}$ by the following argument. The shape of the free surface is given implicitly by analytic function $F(x, y) = 0$ before and after cusping.

We are going to assume that there is a cusp at the origin of the x, y plane as in Fig. 3. We further assume that the cusp $y = x^{3/2}/L^{1/2}$ is in the least degenerate form in a sense made clear by the following considerations. Let $F(x, y) = 0$ describe a cusp and suppose $F(x, y)$ can be developed in a series of powers of x and y. We are thinking that the cusp is a limiting form of an analytic function $F(x, y) = 0$ for smooth surfaces.

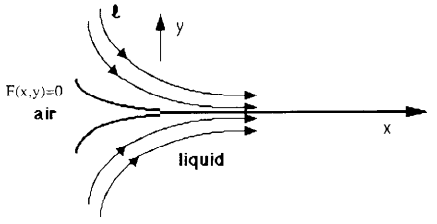

Fig. 3. Flow past a cusp.

Since a cusp is a singular point of the plane curve, the first derivatives vanish at the origin. To have a cusp at the singular point (0, 0) the curve can have only one tangent at (0, 0). Hence, the discriminant of F, $F_{xx}F_{yy} - F_{xy}$, must vanish at (0, 0) and the curvature of the cusp point (0, 0) of $y = y(x)$ is singular. For the coordinates of Fig. 3 this is guaranteed, and is without loss of generality, if $F_{yy} = 1$ and $F_{xy} = 0$. Then the form of the cusp is a balance of third-order terms and y^2 where, to lowest order

$$F(x, y) = F_{yy}(0, 0)y^2 + F_{xxx}(0, 0)x^3 = 0$$

where neglected terms are of the order $x^{7/2}$. Hence to lowest order

$$y = cx^{3/2}, \quad c = \left[-F_{xxx}(0, 0)/F_{yy}(0, 0)\right]^{1/2}$$

The curvature is singular, proportional to $x^{-1/2}$.

The local solution without surface tension given by JNRR (see Section 6) agrees with this, but their local solution with $\sigma \neq 0$ does not. The analytic cusp describes precisely the analytic properties of the global solution of the model Stokes flow problem studied by JM (see Section 8) and the properties put in evidence of the numerical solution of the problem of dip coating given by Palmquist and Kistler [4] (see Section 9). Evidently, surface tension and, not so evidently, short-range molecular forces will keep a true cusp from forming, although an apparent cusp which differs from a true cusp only at molecular dimensions can form. We did not pursue the idea of an analytic cusp, which was presented in our first submission to JFM, because we could not reconcile it with Richardson's solution.

5. Richardson's solution

S. Richardson [3] did an elegant analysis of two-dimensional bubbles in Stokes flow. He proved that the only possible line singularity of the interface between a viscous liquid and an inviscid two-dimensional bubble is a true cusp. For a cusp that opens on the negative x-axis, his expression

for the leading contribution to the stream function, expressed in polar coordinates, is

$$\psi = \frac{\sigma}{2\pi\mu} r \log r \sin \phi \tag{1}$$

here σ is the surface tension coefficient and μ is the viscosity. This formula shows that there is a point force, 2σ, exerted by the free surface on the fluid and that the velocity near the origin is in the negative x-direction. The velocity near the origin is infinite and, perhaps more seriously, the velocity gradient is not square integrable, leading to an infinite amount of energy dissipation. The free surface at leading order simply coincides with the negative x-axis; the actual opening of the cusp would have to be determined from higher-order corrections which are worked out here at lowest order. The main features of cusping cannot be explained by (1), since the velocity of the fluid is in the positive, rather than the negative, x-direction (Fig. 3).

Clearly we may ignore (1) if surface tension $\sigma = 0$, but if $\sigma \neq 0$, and there is a cusp, (1) must be considered. This is because at the cusp the angle of the interface has a jump of 2π, leading to a delta-function singularity in the flow. This point force must be balanced by a singularity in the flow. Lamb [5, p. 607] derived (1) for the problem of a point force acting at the center of a circle and he notes that the solution "... fails to give a definite result..." as the radius of the circle tends to infinity. This means that if there is a cusp, and $\sigma \neq 0$, then Richardson's solution will dominate in the far field.

In the local analysis the behavior for large r is irrelevant and (1) is a large term only in a region of molecular dimension near the cusp tip. In order for the velocity from (1) to be of the same order as U, we must have $\log r \approx 2\pi Ca$. Here it is understood that r is made dimensionless by a geometric length scale. These scales are the only ones available for Stokes flow in which U, σ and μ are the material parameters. A convenient geometric length scale is the distance to the cusp point, slightly larger than the cylinder radius, 1.25 cm. Using 2.5 as a lower bound for Ca, we find that $\log r$ must be on the order of 1.57. From this we conclude that Richardson's solution does not dominate over the macroscopic (approximately uniform) flow until we reach a length scale of approximately 10^{-7} cm (10 Å). Such length scales are far beyond the means of optical observation and actually reach the limits of applicability of continuum mechanics. Van der Waals forces across the air gap between the long arcs at the cusp can be expected to become important already at 1000 Å and the physics of disjoining pressures would then be important long before Richardson's solution acts strongly.

The mathematical difficulties of Richardson's solution never arise because the solution is always analytic with true cusping only when $\sigma = 0$. JM computed this analytic solution for their vortex dipole model. For capillary numbers of the magnitude involved in the experiments of JNRR the cusp is apparent, with rounding on a molecular dimension so that the physical problems generated by losing the usual continuum description of the continuum in terms of surface tension alone are not resolved.

6. Local solutions (Newtonian)

JNRR gave local solutions of the biharmonic equation. The flow is assumed to be a small perturbation of uniform flow with velocity U in the positive x-direction, and the free surface is a small perturbation of the negative x-axis. Let (u, v) denote the perturbations to the velocity and let h denote the position of the free surface that is located above the cusp. We first analyze Newtonian fluids with zero surface tension. We introduce a stream function ψ by

$$u = \psi_y \quad v = -\psi_x. \tag{2}$$

The positive x-axis is a line of symmetry; we first look for antisymmetric stream functions, corresponding to symmetric flow fields. In polar coordinates, we then have the following expression for the stream function

$$\psi = r^{\lambda}\{A \sin(\lambda\phi) + B \sin[(\lambda - 2)\phi]\}; \tag{3}$$

this expression incorporates the desired symmetry. At $\phi = \pi$, we must satisfy the conditions of zero shear and normal stress,

$$u_y + v_x = 0, \qquad 2\mu v_y - p = 0, \tag{4}$$

which can be shown to translate into

$$\begin{aligned} &\frac{1}{r^2}\psi_{\phi\phi} + \frac{1}{r}\psi_r\psi_{rr} = 0, \\ &\frac{3}{r}\psi_{rr\phi} + \frac{1}{r^3}\psi_{\phi\phi\phi} - \frac{3}{r^2}\psi_{r\phi} + \frac{4}{r^3}\psi_{\phi} = 0 \end{aligned} \tag{5}$$

where $(\psi_\phi/r, -\psi_r)$ are the radial and tangential velocity, respectively. We may evaluate (5), using (3), and we find that

$$\begin{aligned} &[\lambda A + (\lambda - 2)B] \sin(\lambda\pi) = 0, \\ &(A + B) \cos(\lambda\pi) = 0. \end{aligned} \tag{6}$$

Clearly, we have non-trivial solutions for $\lambda = 3/2$. The linearization of the kinematic free surface condition leads to

$$Uh' = v = -\psi_x = \psi_r, \tag{7}$$

and hence,

$$h = \frac{1}{U} r^{\lambda}(A + B). \tag{8}$$

Symmetric stream functions (i.e. antisymmetric flows) are given by the expression

$$\psi = r^{\lambda}\{A \cos(\lambda\phi) + B \cos[(\lambda - 2)\phi]\}. \tag{9}$$

In this case, (5) leads to

$$\begin{aligned} &[\lambda A + (\lambda - 2)B] \cos(\lambda\pi) = 0, \\ &(A + B) \sin(\lambda\pi) = 0. \end{aligned} \tag{10}$$

Again, $\lambda = 3/2$ is a solution; in place of (8) we get $h = 0$. Higher-order corrections would be a composition of symmetric and antisymmetric functions like (3) and (9) in a combination determined globally.

7. Local solutions (non-Newtonian)

It may be assumed that if surface tension prevents the formation of a true cusp in Newtonian liquids, it will do the same in non-Newtonian liquids. Therefore, to study cusping we set the surface tension to zero and try for a separated similarity solution in polar form. The appropriate model which perturbs uniform flow is the linearized viscoelastic fluid, which was already considered by JNRR. In this case the Newtonian velocity actually provides a solution even for the viscoelastic cases, with the generic analytic cusp shape $y = cx^{3/2}$. The stresses, however, are now given by

$$T(x, y) = \int_0^{\infty} G(s) A(x - Us, y)\, \mathrm{d}s, \tag{11}$$

where G denotes the stress relaxation function and A is twice the rate of strain tensor. The stresses given by (11) are less singular at the cusp than in the Newtonian case. The linear viscoelastic fluid is a fairly universal form of constitutive equation to which nearly all models will reduce when linearized around uniform flow (see Joseph [6]). However, it appears doubtful whether linear viscoelasticity is very useful in interpreting experiments in non-Newtonian fluids. The extensional behavior of such fluids is highly non-linear, leading to extensional stresses much larger than those in Newtonian fluids with the same shear viscosity. We note that a non-cusped

interface necessarily has a stagnation point, with the associated potential for a build-up of elongational stresses. Cusping gets rid of the stagnation point and alleviates some of these elongational stresses. This effect should favor cusping in non-Newtonian fluids. There are probably not many non-linear models of fluids for which a local analysis like that given in Section 6 can be carried out. The second-order fluid is an exception. For this model the extra stress $\boldsymbol{S} = \boldsymbol{T} + \mathrm{p}\mathbf{1}$ is related to velocity gradients by the expression

$$\boldsymbol{S} = \mu \boldsymbol{A}[\boldsymbol{u}] + \alpha_1 \boldsymbol{B}[\boldsymbol{u}] + \alpha_2 \boldsymbol{A}^2[\boldsymbol{u}], \tag{12}$$

where $\boldsymbol{A} = \boldsymbol{L} + \boldsymbol{L}^{\mathrm{T}}$, $\boldsymbol{L} = \nabla \boldsymbol{u}$ and

$$\boldsymbol{B}[\boldsymbol{u}] = \frac{\partial \boldsymbol{A}}{\partial t} + \boldsymbol{u} \cdot \nabla \boldsymbol{A} + \boldsymbol{A}\boldsymbol{L} + \boldsymbol{L}^{\mathrm{T}}\boldsymbol{A}. \tag{13}$$

This is an asymptotic form for slow, slowly varying or steady motions. Since cusping occurs at stagnation points (as the surface tension goes to zero) where the velocity vanishes, and it can occur when the velocities are very small, we could imagine using it in an analysis of cusping. In fact the use of this equation near a singularity cannot be defended from first principle arguments. I did try it, though, and I was astonished to see that I could carry out the analysis which is given below, leading again to the generic analytic cusp which was introduced from general considerations without dynamics in Section 4. It is well known that plane flow of Newtonian fluids with prescribed velocities on solid walls will satisfy the equations for the same problem of a second-order fluid, but with a different pressure. This is Tanner's theorem, but it does not hold generally for flow with free surfaces on which the traction stress vector vanishes. Residual stresses appear on the free surface. This makes it all the more interesting that the analytic cusp singularity does satisfy the equation of a second-order fluid and it suggests that there is perhaps a wide validity for the argument in Section 4 even in the case of non-Newtonian fluids.

Another reason to consider second-order fluids, presented already in JNRR, is that the mysterious correlation of cusping in non-Newtonian fluids with Newtonian capillary numbers does follow from scalings associated with the second-order fluid, starting with the idea that a controlling parameter ought to be the ratio

$$\frac{\text{elongational stress}}{\text{surface tension stress}}.$$

For this we estimate elongational stresses as $|\alpha_1| U^2/l^2$, where l is a characteristic length, and we estimate stresses resulting from surface tension as σ/l. This leads to the capillary number $Ca = |\alpha_1| U^2/\sigma l$. Next we

estimate l as $U\tau$, where τ is a characteristic time scale, so we have $Ca = |\alpha_1| U/\sigma\tau$. A possible estimate for τ is $|\alpha_1|/\mu$; in this case we obtain the same capillary number as in the Newtonian case. It might be argued, however, that shorter relaxation times could be important. Using such shorter relaxation times for τ would also raise the value of Ca.

If p is the "pressure" in a second-order fluid where $\boldsymbol{T} = -p\mathbf{1} + \boldsymbol{S}$ and $\boldsymbol{S}$ is given by (12), then we can use a result of Giesekus to find an expression for a second-order fluid in plane flow. If

$$\operatorname{div} \boldsymbol{A}^2 = \boldsymbol{\nabla}\Gamma, \tag{14}$$

and

$$\operatorname{div} \boldsymbol{A} = \boldsymbol{\nabla} Q, \tag{15}$$

then

$$\operatorname{div} \boldsymbol{B} = \boldsymbol{\nabla}\left(\Gamma + \boldsymbol{u}\cdot\boldsymbol{\nabla}Q + \tfrac{1}{4}\operatorname{tr} \boldsymbol{A}^2\right), \tag{16}$$

where $\Gamma = \frac{1}{2}\operatorname{tr} \boldsymbol{A}^2$. If inertia can be neglected, then

$$\operatorname{div} \boldsymbol{T} = \operatorname{div}\left(-p\mathbf{1} + \mu\boldsymbol{A} + \alpha_1\boldsymbol{B} + \alpha_2\boldsymbol{A}^2\right) = 0. \tag{17}$$

Using (14–17), we get

$$\boldsymbol{\nabla}\left[-p + \mu Q + \alpha_1(\boldsymbol{u}\cdot\boldsymbol{\nabla})Q + \frac{3\alpha_1}{2}\Gamma + \alpha_2\Gamma\right] = 0. \tag{18}$$

Hence

$$\boldsymbol{T} = -\left[\mu Q + \alpha_1(\boldsymbol{u}\cdot\boldsymbol{\nabla})Q + \frac{3\alpha_1}{2}\Gamma\right]\mathbf{1} + \mu\boldsymbol{A} + \alpha_1\boldsymbol{B}, \tag{19}$$

where the coefficient of α_2 vanishes in plane flow.

Now we are ready for the analysis. We are going to assume a cusp which is a perturbation of uniform motion in the x-direction. Therefore

$$\boldsymbol{u} = -U\boldsymbol{e}_x + v\boldsymbol{e}_r + w\boldsymbol{e}_\phi = \left[-U\cos(\phi) + v\right]\boldsymbol{e}_r + \left[U\sin(\phi) + w\right]\boldsymbol{e}_\phi \tag{20}$$

where v and w are given by the stream function (3),

$$v = \frac{1}{r}\frac{\partial\psi}{\partial\phi} = r^{(\lambda-1)}\{A\lambda\cos(\lambda\phi) + B(\lambda-2)\cos[(\lambda-2)\phi]\} \tag{21}$$

so that v is an even function of ϕ, and

$$w = -\frac{\partial\psi}{\partial r} = -\lambda r^{(\lambda-1)}\{A\sin(\lambda\phi) + B\sin[(\lambda-2)\phi]\}, \tag{22}$$

with the cusp located at $\phi = \pi$. We calculate the stress in the fluid using (19),

$$\boldsymbol{L} = \nabla \boldsymbol{u} = \begin{pmatrix} L_{rr} & L_{r\phi} \\ L_{\phi r} & L_{\phi\phi} \end{pmatrix} \tag{23}$$

where

$$L_{rr} = \frac{\partial v}{\partial r} = (\lambda - 1) r^{(\lambda-2)} \{ A\lambda \cos(\lambda\phi) + B(\lambda - 2) \cos[(\lambda - 2)\phi] \},$$

$$L_{r\phi} = \frac{1}{r}\frac{\partial v}{\partial \phi} - \frac{w}{r} = (1 - \lambda) r^{(\lambda-2)} \{ A\lambda \sin(\lambda\phi) + B(\lambda - 4) \sin[(\lambda - 2)\phi] \}, \tag{24}$$

$$L_{\phi r} = \frac{\partial w}{\partial r} = (1 - \lambda)\lambda r^{(\lambda-2)} \{ A \sin(\lambda\phi) + B \sin[(\lambda - 2)\phi] \},$$

and

$$L_{\phi\phi} = \frac{1}{r}\frac{\partial w}{\partial \phi} + \frac{v}{r} = -L_{rr}.$$

Moreover

$$\boldsymbol{A} = \boldsymbol{L} + \boldsymbol{L}^{\mathrm{T}} = \begin{pmatrix} A_{rr} & A_{r\phi} \\ A_{\phi r} & A_{\phi\phi} \end{pmatrix} \tag{25}$$

where

$$A_{rr} = 2L_{rr},$$

$$A_{r\phi} = A_{\phi r} = L_{r\phi} + L_{\phi r} = r\frac{\partial (w/r)}{\partial r} + \frac{1}{r}\frac{\partial v}{\partial \phi},$$

$$= 2(1 - \lambda) r^{(\lambda-2)} \{ A\lambda \sin(\lambda\phi) + B(\lambda - 2) \sin[(\lambda - 2)\phi] \}, \tag{26}$$

$$A_{\phi\phi} = 2L_{\phi\phi} = -2L_{rr}.$$

It follows that

$$\boldsymbol{A}^2 = \begin{pmatrix} \Gamma & 0 \\ 0 & \Gamma \end{pmatrix} \tag{27}$$

where

$$\Gamma = A_{rr}^2 + A_{r\phi}^2 \tag{28}$$

Next we define

$$\boldsymbol{B} = (\boldsymbol{u} \cdot \nabla)\boldsymbol{A} + \boldsymbol{Z} \tag{29}$$

where

$$\boldsymbol{Z} = \begin{pmatrix} Z_{rr} & Z_{r\phi} \\ Z_{\phi r} & Z_{\phi\phi} \end{pmatrix} = \boldsymbol{AL} + (\boldsymbol{AL})^{\mathrm{T}}. \tag{30}$$

Using the existing definitions we find

$$\begin{aligned} Z_{rr} &= 2(A_{rr}L_{rr} + A_{r\phi}L_{\phi r}), \\ Z_{r\phi} &= Z_{\phi r} = A_{rr}(L_{r\phi} - L_{\phi r}), \\ Z_{\phi\phi} &= 2(A_{r\phi}L_{r\phi} + A_{rr}L_{rr}). \end{aligned} \tag{31}$$

In order to find Q we solve the system,

$$\begin{aligned} \frac{\partial Q}{\partial r} &= \nabla^2 v - \frac{v}{r^2} - \frac{2}{r^2}\frac{\partial w}{\partial \phi} + \frac{1}{r}\frac{\partial v}{\partial r}, \\ \frac{1}{r}\frac{\partial Q}{\partial \phi} &= \nabla^2 w + \frac{2}{r^2}\frac{\partial v}{\partial \phi} - \frac{w}{r^2} + \frac{1}{r}\frac{\partial w}{\partial r}, \end{aligned} \tag{32}$$

where $\nabla^2 = \partial^2/\partial r^2 + 1/r^2\ \partial^2/\partial\phi^2$. Using eqns. (3), (20) and (21) we find

$$\begin{aligned} \frac{\partial Q}{\partial r} &= 4B(\lambda-1)(\lambda-2)r^{(\lambda-3)}\cos[(\lambda-2)\phi] \\ \frac{\partial Q}{\partial \phi} &= -4B(\lambda-1)(\lambda-2)r^{(\lambda-2)}\sin[(\lambda-2)\phi]. \end{aligned} \tag{33}$$

Therefore

$$Q = 4B(\lambda-1)r^{(\lambda-2)}\cos[(\lambda-2)\phi].$$

Now we can look at the stress tensor. We first have the condition that the shear stress at the cusp must be zero. Thus

$$\begin{aligned} T_{r\phi} &= \mu A_{r\phi} + \alpha_1 B_{r\phi} \\ &= \mu\big[(1-\lambda)r^{(\lambda-2)}\{A\lambda\sin(\lambda\pi) + B(\lambda-2)\sin[(\lambda-2)\pi]\} \\ &\quad + \alpha_1\big[-\big(U + r^{(\lambda-1)}\{A\lambda\cos(\lambda\pi) + B(\lambda-2)\cos[(\lambda-2)\pi]\}\big) \\ &\quad \times 2(1-\lambda)(\lambda-2)r^{(\lambda-3)}\{A\lambda\sin(\lambda\pi) + B(\lambda-2)\sin[(\lambda-2)\pi]\} \\ &\quad + \big(-\lambda r^{(\lambda-1)}\{A\sin(\lambda\pi) + B\sin[(\lambda-2)\pi]\}\big) \\ &\quad \times 2(1-\lambda)r^{(\lambda-3)}\big\{A\lambda^2\cos(\lambda\pi) + B(\lambda-2)^2\cos[(\lambda-2)\pi]\big\} \\ &\quad + 2(\lambda-1)r^{(\lambda-2)}\{A\lambda\cos(\lambda\pi) + B(\lambda-2)\cos[(\lambda-2)\pi]\} \\ &\quad \times\big((1-\lambda)r^{(\lambda-2)}\{A\lambda\sin(\lambda\pi) + B(\lambda-4)\sin[(\lambda-2)\pi]\} \\ &\quad - (1-\lambda)\lambda r^{(\lambda-2)}\{A\sin(\lambda\pi) + B\sin[(\lambda-2)\pi]\}\big)\big]. \end{aligned} \tag{34}$$

We also have the condition that the normal stress at the cusp must be zero. We find that

$$
\begin{aligned}
T_{\phi\phi} &= -\mu Q - \alpha_1(\boldsymbol{u}\cdot\boldsymbol{\nabla})Q - \left(\tfrac{3}{2}\alpha_1 + \alpha_2\right)\Gamma + \mu A_{\phi\phi} + \alpha_1 B_{\phi\phi} + \alpha_2 A_{\phi\phi}^2 \\
&= -\mu\big(4B(\lambda-1)r^{(\lambda-2)}\cos[(\lambda-2)\pi] + 2(\lambda-1)r^{(\lambda-2)} \\
&\quad\times\{A\lambda\cos(\lambda\pi) + B(\lambda-2)\cos[(\lambda-2)\pi]\}\big) \\
&\quad+\alpha_1\big[-\big(U + r^{(\lambda-1)}\{A\lambda\cos(\lambda\pi) + B(\lambda-2)\cos[(\lambda-2)\pi]\}\big) \\
&\quad\times\{4B(\lambda-1)(\lambda-2)r^{(\lambda-3)}\cos[(\lambda-2)\pi]\} \\
&\quad+\big(\lambda r^{(\lambda-1)}\{A\sin(\lambda\pi) + B\sin[(\lambda-2)\pi]\}\big) \\
&\quad\times\{-4B(\lambda-1)(\lambda-2)r^{(\lambda-3)}\sin[(\lambda-2)\pi]\} \\
&\quad-\tfrac{3}{2}\big[4\big((\lambda-1)r^{(\lambda-2)}\{A\lambda\cos(\lambda\pi) + B(\lambda-2)\cos[(\lambda-2)\pi]\}\big)^2 \\
&\quad+\big((1-\lambda)r^{(\lambda-2)}\{A\lambda\sin(\lambda\pi) + B(\lambda-2)\sin[(\lambda-2)\pi]\}\big)^2\big] \\
&\quad+\big(U + r^{(\lambda-1)}\{A\lambda\cos(\lambda\pi) + B(\lambda-2)\cos[(\lambda-2)\pi]\}\big) \\
&\quad\times\big(-2(\lambda-1)(\lambda-2)r^{(\lambda-3)}\{A\lambda\cos(\lambda\pi) + B(\lambda-2)\cos[(\lambda-2)\pi]\}\big) \\
&\quad-\big(\lambda r^{(\lambda-1)}\{A\sin(\lambda\pi) + B\sin[(\lambda-2)\pi]\}\big)\big(2(\lambda-1)r^{(\lambda-3)} \\
&\quad\times\big\{A\lambda^2\sin(\lambda\pi) + B(\lambda-2)^2\sin[(\lambda-2)\pi]\big\}\big) \\
&\quad+2\big[\big(2(1-\lambda)r^{(\lambda-2)}\{A\lambda\sin(\lambda\pi) + B(\lambda-2)\sin[(\lambda-2)\pi]\}\big) \\
&\quad\times\big((1-\lambda)r^{(\lambda-2)}\{A\lambda\sin(\lambda\pi) + B(\lambda-4)\sin[(\lambda-2)\pi]\}\big) \\
&\quad+2\big((\lambda-1)r^{(\lambda-2)}\{A\lambda\cos(\lambda\pi) + B(\lambda-2)\cos[(\lambda-2)\pi]\}\big)^2\big]. \qquad (35)
\end{aligned}
$$

If we chose $\lambda = 3/2$, (34) and (35) become respectively

$$
0 = \mu\big\{1 - \lambda r^{(\lambda-2)}[A\lambda + B(\lambda-2)]\big\} \qquad (36)
$$

$$
\begin{aligned}
0 &= \alpha_1\big\{-4B\lambda(\lambda-1)(\lambda-2)r^{(2\lambda-4)}(A+B) - 6(1-\lambda)^2 r^{(2\lambda-4)} \\
&\quad\times[A\lambda + B(\lambda-2)]^2 - 2\lambda(\lambda-1)r^{(2\lambda-4)}(A+B)\big[A\lambda^2 + B(\lambda-2)^2\big] \\
&\quad+4(1-\lambda)^2 r^{(2\lambda-4)}[A\lambda + B(\lambda-2)][A\lambda + B(\lambda-4)]\big\} \\
&= \alpha_1[A\lambda + B(\lambda-2)]r^{(2\lambda-4)}\big(-\lambda^2(\lambda-1)(A+B)6(1-\lambda)^2 \\
&\quad\times[A\lambda + B(\lambda-2)] + 4(1-\lambda)^2[A\lambda + B(\lambda-4)]. \qquad (37)
\end{aligned}
$$

Thus if $[A\lambda + B(\lambda - 2)] = 0$ with $\lambda = 3/2$, both the normal and shear stress conditions are satisfied. Finally we wish to examine T_{rr}. Using the above definitions we find

$$
\begin{aligned}
T_{rr} &= -\mu Q - \alpha_1(\boldsymbol{u}\cdot\nabla)Q - \left(\tfrac{3}{2}\alpha_1 + \alpha_2\right)\Gamma + \mu A_{rr} + \alpha_1 B_{rr} + \alpha_2 A_{rr}^2 \\
&= \mu\big(-4B(\lambda-1)r^{(\lambda-2)}\cos[(\lambda-2)\pi] + 2(\lambda-1)r^{(\lambda-2)}\{\lambda A\cos(\lambda\pi) \\
&\quad + B(\lambda-2)\cos[(\lambda-2)\pi]\}\big) + \alpha_1\big[-\big(U + r^{(\lambda-1)}\{A\lambda\cos(\lambda\pi) \\
&\quad + B(\lambda-2)\cos[(\lambda-2)\pi]\}\big)\{4B(\lambda-1)(\lambda-2)r^{(\lambda-3)}\cos[(\lambda-2)\pi]\} \\
&\quad + \big(\lambda r^{(\lambda-1)}\{A\sin(\lambda\pi) + B\sin[(\lambda-2)\pi]\}\big)\{-4B(\lambda-1)(\lambda-2)r^{(\lambda-3)} \\
&\quad \times\sin[(\lambda-2)\pi]\} - \tfrac{3}{2}\big[4\big((\lambda-1)r^{(\lambda-2)}\{A\lambda\cos(\lambda\pi) + B(\lambda-2) \\
&\quad \times\cos[(\lambda-2)\pi]\}\big)^2 + \big((1-\lambda)r^{(\lambda-2)}\{A\lambda\sin(\lambda\pi) + B(\lambda-2) \\
&\quad \times\sin[(\lambda-2)\pi]\}\big)^2\big] - \big(U + r^{(\lambda-1)}\{A\lambda\cos(\lambda\pi) + B(\lambda-2) \\
&\quad \times\cos[(\lambda-2)\pi]\}\big)\big(-2(\lambda-1)(\lambda-2)r^{(\lambda-3)}\{A\lambda\cos(\lambda\pi) \\
&\quad + B(\lambda-2)\cos[(\lambda-2)\pi]\}\big) + \big(\lambda r^{(\lambda-1)}\{A\sin(\lambda\pi) \\
&\quad + B\sin[(\lambda-2)\pi]\}\big)\big(2(\lambda-1)r^{(\lambda-3)}\big\{A\lambda^2\sin(\lambda\pi) \\
&\quad + B(\lambda-2)^2\sin[(\lambda-2)\pi]\big\}\big) + 2\big[\big((1-\lambda)r^{(\lambda-2)}\{A\lambda\sin(\lambda\pi) \\
&\quad + B(\lambda-2)\sin[(\lambda-2)\pi]\}\big)\big((1-\lambda)\lambda r^{(\lambda-2)}\{A\sin(\lambda\pi) \\
&\quad + B\sin[(\lambda-2)\pi]\}\big) + 2\big((\lambda-1)r^{(\lambda-2)}\{A\lambda\cos(\lambda\pi) \\
&\quad + B(\lambda-2)\cos[(\lambda-2)\pi]\}\big)^2. \qquad (38)
\end{aligned}
$$

$$
\begin{aligned}
T_{rr} &= \alpha_1\big\{-4B\lambda(\lambda-1)(\lambda-2)r^{(2\lambda-4)}(A+B) - 6(1-\lambda)^2 r^{(2\lambda-4)} \\
&\quad \times[A\lambda + B(\lambda-2)]^2 + 2\lambda(\lambda-1)r^{(2\lambda-4)}(A+B)\big[A\lambda^2 + B(\lambda-2)^2\big] \\
&\quad + 2(1-\lambda)^2 r^{(2\lambda-4)}[A\lambda + B(\lambda-2)](A\lambda + B(\lambda-4))\big\} \\
&= \alpha_1\{A\lambda + B[(\lambda-2)]\}r^{(2\lambda-4)}\big\{-6(1-\lambda)^2\big[A\lambda + B(\lambda-2) \\
&\quad + -2(1-\lambda)^2(A+B)\big] + 2\alpha_1\lambda(\lambda-1)r^{(2\lambda-4)}(A+B) \\
&\quad \times\big[A\lambda^2 + B(\lambda-2)(\lambda-4)\big]\big\}. \qquad (39)
\end{aligned}
$$

If $[A\lambda + B(\lambda-2)] = 0$, (39) reduces to

$$
T_{rr} = 2\alpha_1(\lambda-1)r^{(2\lambda-4)}(A+B)\big[A\lambda^2 + B(\lambda-2)(\lambda-4)\big], \qquad (40)
$$

which goes to infinity as $1/r$. The extra tension at the cusp point of a generic analytic cusp on a second-order fluid is unphysically large and leads to an unbounded dissipation of energy.

Nelson and I found that unlike the Newtonian case, there is no singular, local antisymmetric solution which makes the shear and normal stress vanish at a cusp. This means that if there is a local solution with the generic analytic cusp, it is locally symmetric with global antisymmetric parts vanishing strongly, at least like r_1^2 at the cusp tip.

8. Local solution (Newtonian with disjoining pressure)

Whatever you do, with or without surface tension, you find that the arcs of the effective cusp are separated by a variable distance which must decrease to molecular dimensions. There ought to be long arcs, where the separation distance varies from 50 to 1000 Å, for which a local analysis using disjoining pressures of the same nature as are used in the study of film rupture, coalescence and drying (for example, Ruckenstein and Jain [7], Gumerman and Homsy [8], Williams and Davis [9] and DeGennes [10]) makes sense. Because of the simple analytic form of the potential for disjoining pressures

$$\varphi = \hat{A}/h^3(x) \tag{41}$$

where $h(x)$ is the distance between the areas of the cusp at the place x and $\hat{A}$ is the Hamaker constant, the problem of local analysis of cusping is rather easily extended to include the effect of disjoining pressure. In the fluid we must satisfy

$$\left.\begin{aligned} &\mu\nabla^2 u - (p+\phi)_x = 0, \\ &\mu\nabla^2 v - (p+\phi)_x, \\ &u_x + v_y = 0 \end{aligned}\right\} \tag{42}$$

and

$$\left.\begin{aligned} &v = U, \\ &u_y + v_x = 0, \\ &-p + 2v_y = 0 \end{aligned}\right\} \tag{43}$$

on $y = h$, as in Section 6. Let $\hat{\pi} = p + \phi$. The normal stress balance (43) (last equation) becomes

$$-\hat{\pi} + \hat{A}/h^3 + 2v_y = 0 \tag{44}$$

We get $\hat{\pi}$ from the equations using the local solution (3) and we find that

$$[\lambda A + (\lambda - 2)B] \sin \lambda\pi \tag{45}$$

as before and

$$3\lambda(\lambda - 1)(\lambda - 2)(A + B)\frac{\cos \lambda\pi}{r^{3-\lambda}} + \frac{\hat{A}}{r^{3\lambda}} \sin \lambda^3\pi = 0. \tag{46}$$

We can satisfy (45) and (46) if

$3 - \lambda = 3\lambda$

hence

$$\lambda = \tfrac{3}{4}, \tag{47}$$

$$\tfrac{3}{4}A = \tfrac{5}{4}B, \tag{48}$$

and

$$\tfrac{45}{64}(A + B)\ \frac{3\pi}{4} \sin^3 \frac{3\pi}{4} + \hat{A} = 0. \tag{49}$$

This solution is too singular and it uses all of the disposable constants.

Even though the potential of disjoining pressures (Van der Waals forces) is frequently used in applied studies, it is not firmly rooted in experiments where different situations lead to different results. For example, two hydrophobic surfaces immersed in water and then moved together produce a long-range attraction that is one or two orders of magnitude stronger than predicted by van der Waals theory [11]. It might be expected that short-range forces will collapse the cusp, as in film rupturing, and that the geometric object for which a continuum description ought to be sought has strongly curved arcs, like a tiny sphere, rather than two nearly parallel planes. This is exactly the situation to which the analysis of surface tension in the solution of JM, given next, leads. Since the radius of curvature of that solution is of exponential order, leading to molecular dimensions, the surface tension theory breaks down but it may still be possible to find some form of continuum description. This type of thought may have been in the mind of Rayleigh when he wrote [12] "...the walls of a moderately small cavity certainly tend to collapse with a force measured by the constant surface tension of the liquid. The pressure in the cavity is first proportional to the surface tension and to the curvature of walls. If this law held without limit, the consideration of an infinitely small cavity shows that the intrinsic pressure would be infinite in all liquids. Of course, the law really changes when the dimensions of the cavity are of the same order as the range of attractive forces, and the pressure in the cavity approaches a limit."

We may ask how the pressure approaches its limiting value and what this value might be.

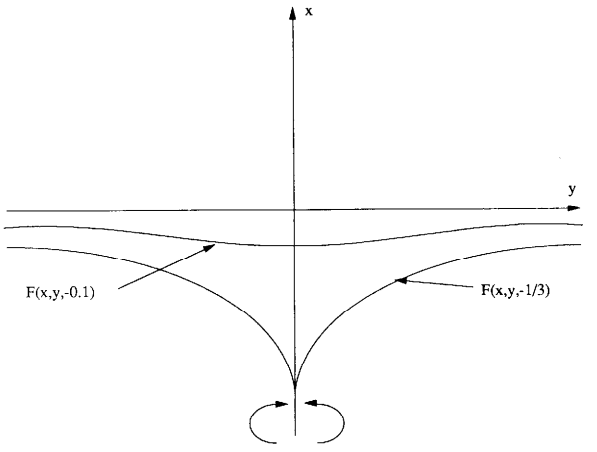

Fig. 4. Diagram of the solution (50) of Jeong and Moffatt [2], showing analytic cusping of $F(x, y, a) = 0$. There is a vortex dipole at $(x, y) = (-d, 0)$.

9. Model problem of Jeong and Moffatt [2]

Jeong and Moffatt solve an idealized model of an experiment in which two cylinders are counter-rotated at low Reynolds number about parallel horizontal axes below the free surface of a viscous fluid. Above a certain critical angular velocity Ω_c, the free surface dips downward and a cusp forms. In their model problem the cylinders are represented by a vortex dipole (Fig. 4) and the solution is obtained by the complex variable techniques which were adapted from elasticity to Stokes flow by Richardson [3]. Surface tension effects are included, but gravity is neglected. Their solution is analytic, with a generic analytic cusp in the limit of zero surface tension. They find that the free surface is given by

$$F(x, y) = y^2 x - (2a - x)(x + a + 1)^2 = 0 \tag{50}$$

where a is a complicated function of the capillary number and is such that

$$a + \tfrac{1}{3} \approx \tfrac{32}{9}\exp(-2\pi Ca) \text{ as } a \to -\tfrac{1}{3} \tag{51}$$

A generic analytic cusp appears in the limit $Ca \to \infty$. Here $Ca = U\mu/\sigma$ where $U = 16\alpha/d^2$ and α, d are parameters used by JM. The capillary number used by JM is 16 times this one and U is actually the streaming velocity past the cusp when $a = -1/3$.

If we put

$$\epsilon = \tfrac{32}{9}\exp(-2\pi Ca) \tag{52}$$

and set

$$a = -\tfrac{1}{3} + \epsilon, \qquad X = x + \tfrac{3}{2} \tag{53}$$

for small ϵ, then to lowest order in ϵ, (52) becomes

$$\tfrac{2}{3}y^2 = X(X^2 - 3\epsilon^2) \tag{54}$$

JM note that this may be put into a universal form

$$\zeta^2 = \tfrac{3}{2}\eta(\eta + 3)^2 \tag{55}$$

where $y = \epsilon^{3/2}\zeta$, $X = \epsilon\eta$. The curve (55) exhibits parabolic behavior $\zeta^2 = 27/2\eta$ for $\eta \ll 1$, and the cuspidal behavior $\zeta^2 \approx 3/2\eta^3$ for $\eta \gg 1$. The points of inflexion at $(\eta, \zeta) = (1, \pm 2\sqrt{6})$ mark the transition between these two regimes.

Though the solution given by JM is analytic and the free surface is smooth when Ca is finite, the radius of curvature R on the line of symmetry on the free surface is given asymptotically by

$$R \approx \tfrac{256}{3}\exp(-2\pi Ca)d \tag{56}$$

where d is the vertical distance of the vortex dipole from the free surface and $Ca = U\mu/\sigma$ with U defined according to our earlier understanding. When $Ca = 4$, $R/d \approx 10^{-9}$ so if d is say of the order of centimeters, R is of the order of angstroms. If $Ca = 16$, then $R/D \approx 1.87 \times 10^{-42}$. This extraordinary behavior implies that it follows then that at capillary numbers of the order of unity the usual continuum description based on surface tension must break down and for capillary numbers, say in excess of 4, the continuum approximation must fail. Certainly this exponential behavior implies the appearance of an apparent cusp at some vaguely defined threshold of capillary numbers of the order of those listed in Table 1. JM note that "...the similarity solution for cusp flow given by JNRR gave a cusp of the form $y \approx Cx^{\lambda}$ where λ is a function (12) of Ca tending to 3/2 as $Ca \to \infty$. Our exact solution of the vortex dipole problem gives $\lambda = 3/2$ even for finite Ca...; this means that the flow in the immediate neighborhood of the cusp (i.e. the parabolic region) has an important effect on the cuspidal region where $y \approx cx^{3/2}$ is still valid".

10. Numerical simulation of Palmquist and Kistler [4]

Palmquist and Kistler [4] studied a liquid film plunging into a pool. They analyze, by means of a finite-element technique, various phenomena that arise in this flow, in particular the formation of a cusp-like corner when the wall is moving sufficiently fast. They also draw analogies between cusp formation where a large liquid body merges with a thin liquid film and

dynamic wetting where a liquid body advances over a previously dry solid. In the latter case, there is a limiting capillary number at which the dynamic contact angle, when measured through the displaced air phase, reaches 0° and the free surface appears to form a cusp with the solid wall.

The key idea in the numerical simulations by Palmquist and Kistler [4] is the assumption that, on a sufficiently small scale, the interface remains smoothly curved and, thus, incorporates a stagnation point. This assumption excludes a priori the formation of a considerable mesh refinement; the computations yield meniscus profiles which exhibit a cusp-like singularity on a visible length scale. At the onset of cusp formation, the calculated profiles of the plunging film and the interface capping the pool appear to meet at a corner with a measurable angle rather than a genuine cusp. Palmquist and Kistler [4] call this corner an apparent cusp. Their computations suggest that the apparent cusp approaches a true cusp in the limit of high capillary numbers, but their finite-element discretization breaks down before this limit is reached.

For Newtonian liquids, the computed solutions replicate the experimental observations of JNRR. In both experiment and theory, the transition from a smooth depression in the pool surface towards a deep cusp is gradual, yet there is a distinct threshold speed at which the interface appears to be sharply pointed. At low and moderate values of Stokes number, which is defined as

$$St \equiv \frac{\rho g H_0^2}{\mu U}, \tag{57}$$

where H_0 is the pre-metered thickness of the liquid film, the critical capillary number is near $Ca_{\text{cusp}} = 2.5$, which is very close to the values measured by JNRR for several Newtonian liquids.

In the finite-element results, the threshold in capillary number arises because, near the onset of apparent cusp formation, the local meniscus curvature at the stagnation point increases exponentially with further increases in Ca, as in the work of JM. The exact value of the critical capillary number Ca_{cusp} is, of course, sensitive to the length scale that is chosen to measure the sharpness of the apparent corner in the computed solution, or the magnification that can be achieved in the experimental observations. Because of the exponential increase in meniscus curvature, however, the sensitivity is small, and good agreement between theory and experiments is obtained without precisely defining the smallest scale that is being resolved. In the finite-element computations, the exponential increase in curvature leads to a failure of the discretization to resolve the local meniscus shape at capillary numbers not much higher than those at the onset of macroscopically apparent cusp formation.

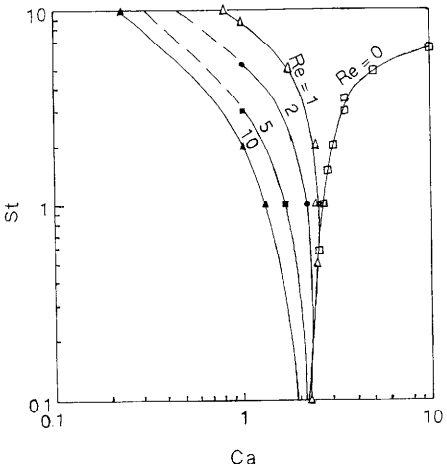

Fig. 5. (Palmquist and Kistler, ref. 4.) Critical values for apparent cusp formation in a Stokes number, capillary number plane, with inertia (Reynolds number) as a parameter.

The critical capillary number Ca_{cusp} is, furthermore, influenced by inertia and gravity effects, and can deviate substantially from $Ca_{\text{cusp}} \approx 2.5$. Palmquist and Kistler [4] used their finite-element algorithm to explore systematically the parameter space with a continuation method. Figure 5 summarizes the limit of apparent cusp formation in an operating plane of St vs. Ca. At low Stokes numbers, i.e. when the viscous drag of the plunging film dominates over gravity effects, the critical capillary number is near $Ca_{\text{cusp}} \approx 2.5$, and is fairly insensitive to Reynolds number which is defined here as

$$Re \equiv \frac{\rho U H_0}{\mu}. \tag{58}$$

In this regime, the apparent cusp is deep and sharply pointed. Towards higher Stokes numbers, however, inertia effects play a key role. In the limit of creeping flow ($Re \ll 1$), Ca_{cusp} increases with St, and the apparent cusp twists in the horizontal direction and becomes less deep and less pointed. Eventually, when gravity dominates over viscous effects at large Stokes numbers, the interface no longer forms a cusp, even when Ca becomes large. Instead, it forms a smoothly curved, standing crest similar to that first predicted by Hansen [13] (see ref. 4 for further comments on this regime). When $Re \geq 0(1)$, on the other hand, cusp formation persists up to very large Stokes numbers. In fact, inertia effects promote very deep and sharply pointed cusps, and Ca_{cusp} can drop well below 2.5. The finite-element results indicate that, near the critical Stokes number above which no

cusp forms for $Re \gg 1$, the recirculating eddy that separates the plunging film flow from the stationary wall shrinks and the stagnation line moves away from the depression in the free surface. This finding suggests that the presence of a stagnation line, and subambient pressure and high deformation rates associated with the flow nearby, are necessary conditions for apparent cusp formation.

The simulations of Palmquist and Kistler [4] are consistent with the analysis of JM; there is an apparent cusp associated with an exponential decrease in the radius. The exponential decrease in the threshold conditions found in the simulation are in good agreement with the experiments of JNRR. They show that the threshold depends on factors other than the capillary number; on gravity and on inertia to name but two. They note that the appearance of a true cusp at high Ca could be impaired by air entrainment and molecular forces that operate at the small distance generated by apparent cusping.

Acknowledgments

This work was supported by the National Science Foundation, the Department of Energy, the Army Research Office and AHPCRC. I wish to thank John Nelson for his help with the calculation in Section 7.

References

1 D.D. Joseph, J. Nelson, M. Renardy and Y. Renardy, Two-dimensional cusped interfaces, J. Fluid Mech., 223 (1991) 383–409.
2 J.T. Jeong and K. Moffatt, Free surface cusps associated with flow at low Reynolds number, J. Fluid Mech., in press (to appear August 1992).
3 S. Richardson, Two-dimensional bubbles in slow flow, J. Fluid Mech., 33 (1968) 475–493.
4 K.E. Palmquist and S.F. Kistler, Formation of cusped interface by liquid film plunging into pool, submitted for publication to J. Fluid. Mech.
5 H. Lamb, Hydrodynamics, 6th edn., Dover, 1932.
6 D.D. Joseph, Fluid dynamics of viscoelastic liquids, Springer, 1990.
7 E. Ruckenstein and R.K. Jain, Spontaneous rupture of thin liquid films, J. Chem. Soc., Faraday Trans. II, 70 (1974) 132–147.
8 R.J. Gumerman and G.M. Homsy, The stability of radially bounded thin film, Chem. Eng. Commun. 2 (1975) 27–36.
9 M.B. Williams and S.H. Davis, Nonlinear theory of film rupture, J. Colloid Interface Sci., 90 (1982) 220–228.
10 P.G. de Gennes, Wetting: statics and dynamics, Rev. Mod. Phys., 57 (1985) 827–863.
11 Y. Tsao, S.X. Yang, D.F. Evans and H. Wennerstöm, Interactions between hydrophobic surfaces. The dependence on temperature and alkyl chain length, Langmuir, in press.
12 F. Rayleigh, On the theory of surface forces, Philos. Mag., 34 (1890) 285–298; 456–475.
13 E.B. Hansen, Stokes flow down a wall into an infinite pool, J. Fluid Mech., 178 (1987) 243–251.